ADVANCED MATERIALS
www.advmat.de

Anomalous High-Temperature Superconductivity in YH_6

Ivan A. Troyan, Dmitrii V. Semenok, Alexander G. Kvashnin,* Andrey V. Sadakov, Oleg A. Sobolevskiy, Vladimir M. Pudalov, Anna G. Ivanova, Vitali B. Prakapenka, Eran Greenberg, Alexander G. Gavriliuk, Igor S. Lyubutin, Viktor V. Struzhkin, Aitor Bergara, Ion Errea, Raffaello Bianco, Matteo Calandra, Francesco Mauri, Lorenzo Monacelli, Ryosuke Akashi, and Artem R. Oganov**

Dedicated to the memory of G. M. Eliashberg

Pressure-stabilized hydrides are a new rapidly growing class of high-temperature superconductors, which is believed to be described within the conventional phonon-mediated mechanism of coupling. Here, the synthesis of one of the best-known high-T_C superconductors—yttrium hexahydride $Im\bar{3}m$-YH_6 is reported, which displays a superconducting transition at ≈224 K at 166 GPa. The extrapolated upper critical magnetic field $B_{c2}(0)$ of YH_6 is surprisingly high: 116–158 T, which is 2–2.5 times larger than the calculated value. A pronounced shift of T_C in yttrium deuteride YD_6 with the isotope coefficient 0.4 supports the phonon-assisted superconductivity. Current–voltage measurements show that the critical current I_C and its density J_C may exceed 1.75 A and 3500 A mm^{-2} at 4 K, respectively, which is higher than that of the commercial superconductors, such as NbTi and YBCO. The results of superconducting density functional theory (SCDFT) and anharmonic calculations, together with anomalously high critical magnetic field, suggest notable departures of the superconducting properties from the conventional Migdal–Eliashberg and Bardeen–Cooper–Schrieffer theories, and presence of an additional mechanism of superconductivity.

Room-temperature superconductivity has been an unattainable dream and subject of speculative discussions for a long time, but times change. The theoretical prediction of record high-temperature superconductor LaH_{10}[1] followed by the experimental confirmation of its critical temperature $T_C \approx 250$–260 K,[2–4] and the discovery of the highest known T_C of 288 K at ≈275 GPa in the ternary carbonaceous sulfur hydrides CSH_x,[5] have opened a new field in high-pressure physics devoted to the investigation of superconducting metal hydrides. Recent successful synthesis of previously predicted superconducting BaH_{12},[6] ThH_{10},[7,8] UH_7 and UH_8,[9] CeH_9,[10] PrH_9,[11] and NdH_9[12] motivated us to perform an experimental study of the Y–H system to find previously predicted potential room-temperature superconductor $Im\bar{3}m$-YH_6, stable in the pressure range between 110 and 300 GPa.[1,13,14]

Dr. I. A. Troyan, Dr. A. G. Ivanova, Dr. A. G. Gavriliuk, Dr. I. S. Lyubutin
Shubnikov Institute of Crystallography
Federal Scientific Research Center Crystallography and Photonics
Russian Academy of Sciences
59 Leninskii Prospect, Moscow 119333, Russia
E-mail: itrojan@crys.ras.ru

D. V. Semenok, Dr. A. G. Kvashnin, Prof. A. R. Oganov
Skolkovo Institute of Science and Technology
Skolkovo Innovation Center
3 Nobel Street, Moscow 121025, Russia
E-mail: A.Kvashnin@skoltech.ru; A.Oganov@skoltech.ru

Dr. A. V. Sadakov, Dr. O. A. Sobolevskiy, Prof. V. M. Pudalov
P.N. Lebedev Physical Institute
Russian Academy of Sciences
Moscow 119991, Russia

Prof. V. M. Pudalov
National Research University
Higher School of Economics
Moscow 101000, Russia

The ORCID identification number(s) for the author(s) of this article can be found under https://doi.org/10.1002/adma.202006832.

DOI: 10.1002/adma.202006832

Prof. V. B. Prakapenka, Dr. E. Greenberg
Center for Advanced Radiation Sources
The University of Chicago
5640 South Ellis Avenue, Chicago, IL 60637, USA

Dr. A. G. Gavriliuk
Institute for Nuclear Research
Russian Academy of Sciences
Fizicheskaya str. 27, Troitsk, Moscow 108840, Russia

Dr. V. V. Struzhkin
Center for High Pressure Science and Technology Advanced Research
Shanghai 201203, China

Prof. A. Bergara, Prof. I. Errea, Dr. R. Bianco
Centro de Física de Materiales CFM
CSIC-UPV/EHU
Paseo Manuel de Lardizabal 5, Basque Country, Donostia 20018, Spain

Prof. A. Bergara
Departamento de Física de la Materia Condensada
University of the Basque Country (UPV/EHU)
Basque Country, Bilbao 48080, Spain

Prof. A. Bergara, Prof. I. Errea
Donostia International Physics Center (DIPC)
Manuel Lardizabal pasealekua 4, Basque Country, Donostia 20018, Spain

The outstanding superconducting properties combined with a relatively low predicted stabilization pressure of about 110 GPa[13] make yttrium hexahydride very interesting. Starting from 2015, the stability field, and physical properties of YH_6, having a sodalite-like crystal structure similar to another predicted hexahydride $Im\bar{3}m$-CaH_6, have been studied in several works.[1,13,14] In 2015, Li et al.[13] have predicted the stability of $Im\bar{3}m$-YH_6 at pressures over 110 GPa. Solving the Migdal–Eliashberg (ME) equations numerically, they found a superconducting transition temperature T_C = 251–264 K at 120 GPa (with the Coulomb pseudopotential μ^* = 0.1–0.13), with the electron–phonon coupling (EPC) coefficient λ reaching 2.93. In the study of the physical properties and superconductivity of $Im\bar{3}m$-YH_6 by Heil et al. in 2019,[15] the most detailed so far, the calculations were made using the fully anisotropic ME theory (as implemented in the EPW code) with Coulomb corrections. They have found that an almost isotropic superconducting gap in YH_6 is caused by a uniform distribution of the coupling over the states of both Y and H sublattices and have predicted the critical temperature T_C = 290 K at 300 GPa.[15] A summary of the previous results of theoretical studies of $Im\bar{3}m$-YH_6 is shown in Table S4 and Figure S12 in the Supporting Information.

Following theoretical predictions, in this work we report an experimental study of the superconducting properties of yttrium hexahydride $Im\bar{3}m$-YH_6, synthesized together with YH_7 and YH_4, after laser-heating yttrium samples compressed to 166–172 GPa in the ammonia borane (NH_3BH_3) medium in the diamond anvil cells. In this work, we focused on the experimental verification of stability and superconductivity of $Im\bar{3}m$-YH_6 and on the calculation of some physical properties that have not been analyzed before.

The high-pressure synthesis was carried out with ammonia borane as a source of hydrogen, following the technique that has shown good results in previous studies.[2,3,7,11,12] We prepared three diamond anvil cells (DACs) with 50 μm culets (K1, M1, and M3), where pure yttrium metal was loaded into sublimated ammonia borane and compressed to 166–172 GPa. The pulsed laser heating technique was used to heat samples at 2400 K (10^5 pulses, 1 μs pulse width, 10 kHz), which resulted in the formation of three compounds $Im\bar{3}m$-YH_6 and YH_4 or YH_{7+x} in all DACs.

The results of the synthesis are strongly dependent on pressure and temperature conditions. In DACs K1 and M1 (the X-ray diffraction (XRD) patterns are shown in **Figure 1** and Figures S7 and S8, Supporting Information), the laser heating of the samples at 166 GPa yielded a complex mixture of products with predominant $Im\bar{3}m$-YH_6 and, probably, $P1$-YH_7 or pseudocubic $Imm2$-YH_7 (Figure S7, Supporting Information), which have been found using the USPEX structure search.[16–18]

At higher pressures (172–180 GPa, DAC M3), a much simpler XRD pattern was observed (Figure 1c,d), with peaks only from the $Im\bar{3}m$-YH_6 and distorted $I4/mmm$-YH_4 phases. The experimental lattice parameters and volumes of synthesized $Im\bar{3}m$-YH_6 are given in **Table 1** (for YH_4 and YH_7, see Table S3, Supporting Information). All Y– H phases were also theoretically examined for the dynamical and mechanical stability according to the Born criteria[19] ($C_{11} - C_{12} > 0$, $C_{11} + 2C_{12} > 0$, $C_{44} > 0$ for cubic phases), the obtained results are presented in Tables S9–S11 in the Supporting Information.

To estimate the thermodynamic stability and the possibility of formation of these hydrides at the experimental pressure–temperature conditions, we carried out searches for stable Y–H compounds using the evolutionary algorithm USPEX[16,17,20] at 150, 200, 250, and 300 GPa. The results of the predictions at 0, 500, 1000, and 2000 K (with the zero-point energy (ZPE) included at the harmonic level) and a pressure of 150 GPa are shown in **Figure 2** (for other pressures, see Figures S2–S6, Supporting Information).

At 150 GPa and 0 K, with the ZPE contribution taken into account, the only stable hydrides are $Fm\bar{3}m$-YH and YH_3, $I4/mmm$-YH_4, $P1$-YH_7 ($Imm2$-YH_7 is a bit less stable), and pseudohexagonal $P\bar{1}$-YH_9, whereas $Im\bar{3}m$-YH_6 is metastable, lying 30 meV per atom above the convex hull (Figure 2a). The distorted hydrogen sublattice in $P\bar{1}$-YH_9 leads to a lower enthalpy of formation compared with previously proposed $P6_3/mmc$-YH_9,[21] which has an ideal hexagonal structure (Figure S1, Supporting Information). The cubic modification of YH_9 with space group $F\bar{4}3m$ (isostructural with PrH_9)[11] is also more stable than $P6_3/mmc$-YH_9[21] (Figure 2a).

As temperature rises, YH_7 loses stability and at 2000 K is 100 meV/atom above the convex hull (Figure 2d). Laser heating of the samples above 1000 K (Figure 2c) leads to the stabilization of $Im\bar{3}m$-YH_6 and transformation of the pseudohexagonal $P\bar{1}$-YH_9 to the cubic modification of YH_9, which becomes stable at temperatures above 1500 K (Figure 2d). Calculations at

Table 1. Experimental (a, V) and predicted (a_{DFT}, V_{DFT}) lattice parameters and unit cell volumes of $Im\bar{3}m$-YH_6 (Z = 2).

DAC	Pressure [GPa]	a [Å]	V [Å^3]	a_{DFT} [Å]	V_{DFT} [Å^3]
M1	166	3.578(3)	45.82	3.573	45.62
K1	168	3.582(3)	45.91	3.565	45.31
M3	172	3.571(2)	45.53	3.557	45.02
M3	177	3.565(9)	45.34	3.551	44.79
M3	180	3.559(8)	45.07	3.546	44.58

Prof. I. Errea
Fisika Aplikatua 1 Saila
University of the Basque Country (UPV/EHU)
Europa plaza 1, Donostia 20018, Spain
Prof. M. Calandra
Departimento di Fisica
Università di Trento
Via Sommarive 14, Povo 38123, Italy
Prof. M. Calandra
Sorbonne Université
CNRS
Institut des Nanosciences de Paris
UMR7588, Paris F-75252, France
Prof. M. Calandra, Dr. F. Mauri, Dr. L. Monacelli
Graphene Labs
Fondazione Istituto Italiano di Tecnologia
Via Morego, Genova I-16163, Italy
Dr. F. Mauri, Dr. L. Monacelli
Dipartimento di Fisica
Università di Roma Sapienza
Piazzale Aldo Moro 5, Roma I-00185, Italy
Prof. R. Akashi
Department of Physics
University of Tokyo
7-3-1 Hongo, Bunkyo, Tokyo 113-8654, Japan

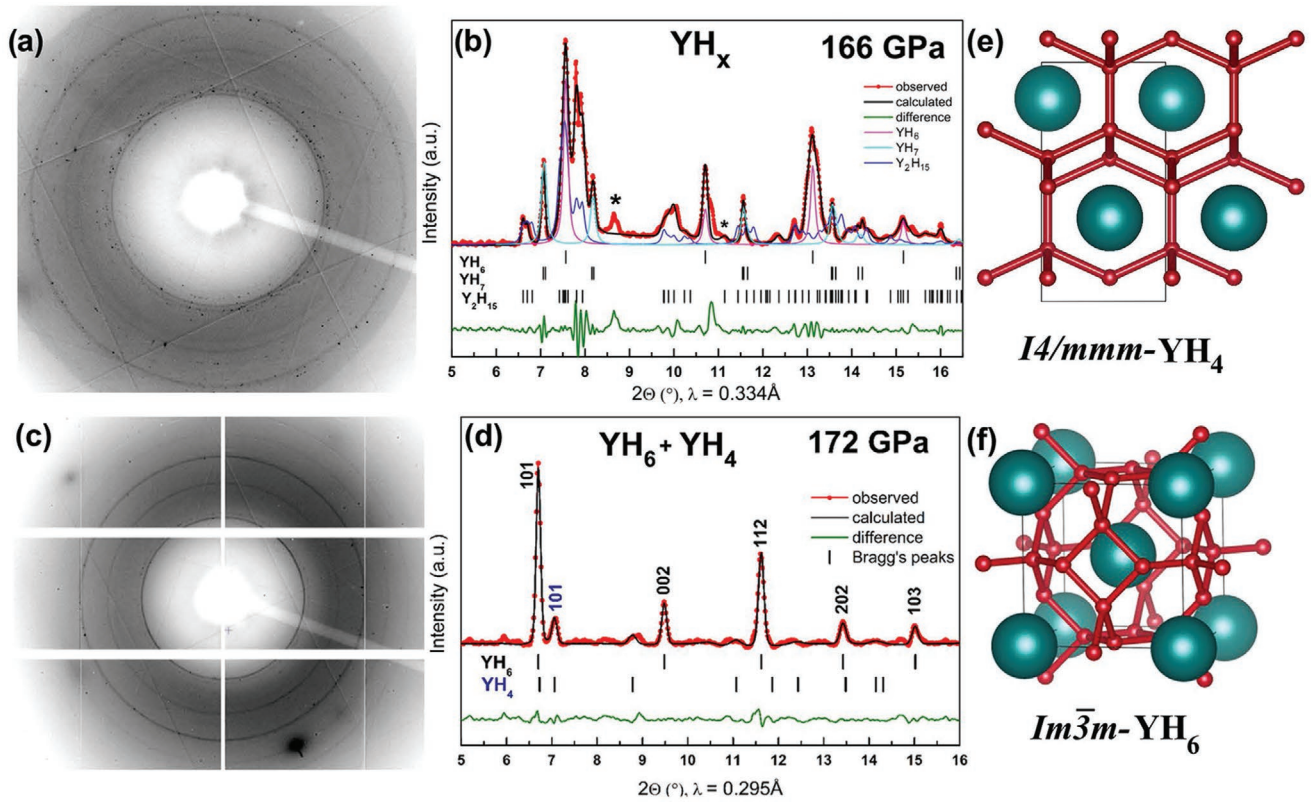

Figure 1. a) XRD pattern of the sample in DAC K1 at 166 GPa collected at a wavelength λ = 0.334 Å. b) Le Bail refinements of $Im\bar{3}m$-YH_6, $Imm2$-YH_7, and $P1$-YH_{7+z} (z = ±0.5) at 166 GPa. Unidentified reflections are marked by asterisks. c) XRD pattern of the M3 sample at 172 GPa collected with λ = 0.295 Å. d) Le Bail refinements of $Im\bar{3}m$-YH_6 and $I4/mmm$-YH_4. The experimental data, fitted line, and residues are shown in red, black, and green, respectively. e,f) Crystal structures of YH_4 and YH_6.

200 and 250 GPa (Figures S5 and S6, Supporting Information) show that both $P1$-YH_7 and $Im\bar{3}m$-YH_6, which below 150 GPa is a metastable "frozen" phase, can form simultaneously, in accordance with the experimental data. In contrast to early predictions,[1,13,14] our computations, considering $P1$-YH_7 and $P\bar{1}$-YH_9, show that yttrium hexahydride stabilizes at 100–150 GPa only due to the entropy factor.

It is interesting that $Fm\bar{3}m$-YH_{10} is thermodynamically metastable at 200–250 GPa and 0–2000 K, with the Gibbs free energy of formation at least 18 meV per atom above the convex hull because of the existence of YH_9 (Figures S5 and S6, Supporting Information). This may explain the failure to synthesize $Fm\bar{3}m$-YH_{10} at 243 GPa.[21] On the other hand, the stabilization of $F\bar{4}3m$-YH_9 may shed light on the recent detection of superconductivity in YH_x at 256–262 K by the group of Dias.[22]

To measure the superconducting transition temperature of synthesized yttrium hexahydride, all DACs were equipped with four Ta/Au electrodes. We used the DACs with a 50 µm culet beveled to 300 µm at 8.5°. Four Ta electrodes (≈200 nm thick) with a gold plating (≈80 nm) were sputtered on the diamond anvil. The composite gaskets consisting of a tungsten ring and a CaF_2/epoxy mixture were used to isolate the electrical leads. To measure the isotope effect in YD_6, a similar cell D1 loaded with ND_3BD_3 was prepared.

An yttrium sample with a thickness of ≈1–2 µm was sandwiched between the electrodes and ammonia borane in the gasket hole with a diameter of 20 µm. In the DAC M3, the electrodes were in short-circuit with the tungsten gasket, therefore no resistivity measurements were made. The temperature dependence of the resistance is shown in **Figure 3**.

Two slightly different superconducting transitions in YH_6 with T_C of 224 K (Figure 3a) and 218 K (Figure 3b) were observed in DACs K1 and M1, respectively. In the K1 cell, the electrical resistance dropped sharply to zero (from 50 mΩ to 5 µΩ, with $\Delta T_C \approx$ 1–2 K) due to good location of the sample, whereas in the M1 cell the electrical resistance did not disappear completely because of the presence of additional phases (Figure S7, Supporting Information). An increase in the pressure from 170 to 200 GPa in the DAC P1 (**Table 2**) leads to a decrease in the critical temperature of YH_6 with a slope dT_C/dP = –0.17 K GPa^{-1} (Figure S15, Supporting Information).

Table 2. Experimental parameters of the DACs.

DAC	Pressure [GPa]	Gasket	Sample size [µm]	Composition/load
K1	166	CaF_2/epoxy	10	Y/NH_3BH_3
M1	165	CaF_2/epoxy	12	Y/NH_3BH_3
M3	172	CaF_2/epoxy	9	Y/NH_3BH_3
D1	172	CaF_2/epoxy	15	Y/ND_3BD_3
P1	170–200	CaF_2/epoxy	19	Y/NH_3BH_3

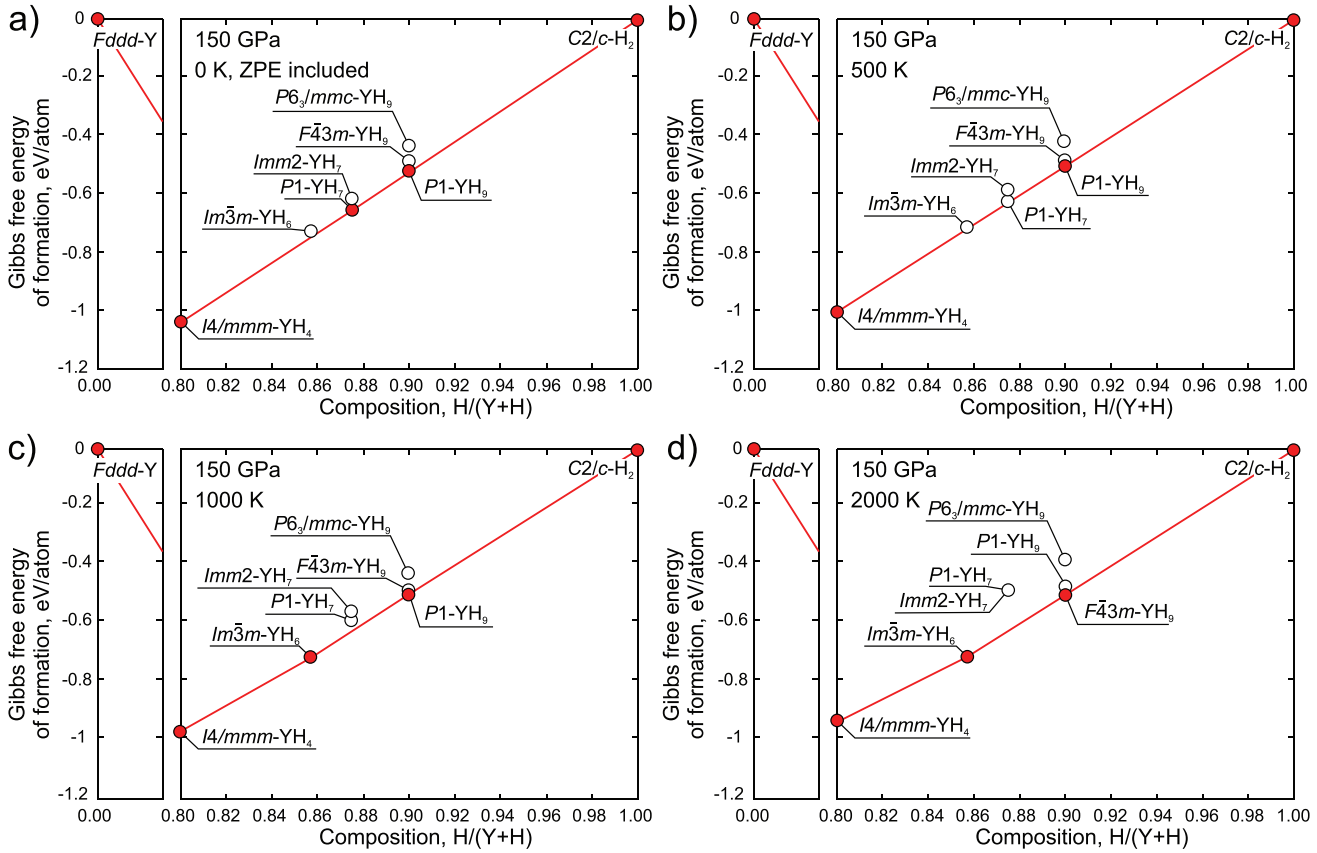

Figure 2. a–d) Calculated convex hulls of the Y–H system at 150 GPa and 0 K (a), 500 K (b), 1000 K (c), and 2000 K (d). The open circles mark metastable phases, the red filled circles correspond to thermodynamically stable phases. The red line is the thermodynamic convex hull of the Y–H system.

The YD_6 sample (DAC D1, Table 2) synthesized using deuterated ammonium borane demonstrates superconducting transition at 170 K (Figure 3a), which corresponds to the isotope coefficient $\alpha_{exp} = 0.4$, lower than the BCS theory gives (≈0.5).

The analysis of the electronic and superconducting properties of the tetragonal YH_4 and pseudocubic *Imm*2-YH_7 shows that the *I*4/*mmm*-YH_4 is a metal with a significantly lower calculated critical temperature (≤115 K) compared with YH_6. Another possible product of the synthesis in DAC M1, *Imm*2-YH_7, has a pronounced pseudogap in the electronic density of states $N(E)$, leading to quite a low density of states at the Fermi level $N(E_F)$, and, as a result, low predicted T_c of 36–46 K (Table S5, Figure S18, Supporting Information). Other possible phases of YH_7, such as *Cc* or *P*1, have even lower $N(E_F)$ and T_C. Thus, none of these phases, except YH_6, can explain the observed superconducting transition at 224–226 K.

In YH_6, the dependence of the T_C (YH_6) on the magnetic induction $B = \mu_0 H$ was measured at 183 and 200 GPa in the range of 0–16 T (Figure 3c,d and Figure S16, Supporting Information) and extrapolated using the Ginzburg–Landau[23] and the Werthamer–Helfand–Hohenberg (WHH)[24] models simplified by Baumgartner et al.[25] Around 200 K, an almost linear dependence of the $T_C(B)$ with a gradient $dB_{c2}/dT \approx -1$ T K^{-1} was observed (Figure 3f). Surprisingly, we found that in YD_6 the dB_{c2}/dT keeps almost the same value –1 T K^{-1} which yields in unexpectedly large extrapolated upper critical field $\mu_0 H_{c2}(0)$ about 114 T (Figure S13, Supporting Information). The extrapolated value of $\mu_0 H_{c2}(0)$ for YH_6 is 116–158 T at 183 GPa, in agreement with the results of Kong et al.[21] These data allow us to estimate $N(E_F)(1 + \lambda)$ factor in the interpolation formula proposed by Carbotte[26] for the $B_{c2}(0)$ of conventional superconductors (works well for H_3S[27] and LaH_{10} ,[2,3] Table S5, Supporting Information) at 7.2–13.3 eV^{-1} f.u.$^{-1}$.

One of the distinguishing features of superconductors is the existence of an upper limit of the current density (J_C) at which superconductivity disappears. The critical currents and the voltage–current (V–I) characteristics for the YH_6 sample were investigated in the range of 10^{-4} to 10^{-2} A in external magnetic fields after further compression to 196 GPa (**Figure 4**a,b). The critical current density was estimated on the basis of the facts that the size of the sample cannot exceed the size of the culet (50 µm), and the thickness of the sample is smaller than the thickness of the gasket before the cell is loaded, ≈10 µm. A zero-field cooling shows that the critical current density in YH_6 exceeds 2×10^7 A m^{-2} at $T = 190$ K which points to the bulk nature of superconductivity. To compare critical currents in magnetic fields at low temperatures, we used a single vortex model. Critical current density in magnetic fields may be defined as the current that creates strong enough force to de-pin a vortex or a bundle of vortices. There are two possible sources of pinning: nonsuperconducting (normal) particles embedded in the superconducting matrix leading to a scattering of electrons, so-called "dl-pinning," or pinning provided

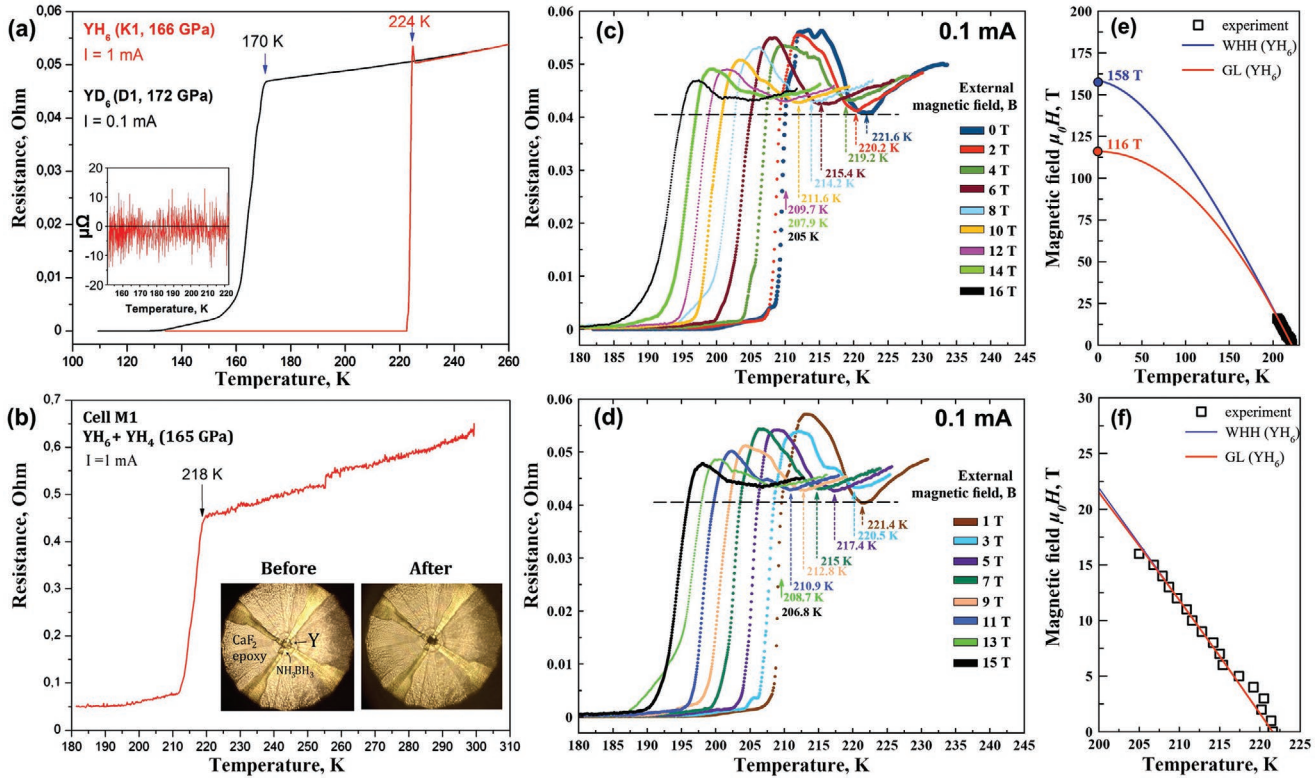

Figure 3. Superconducting transitions in the $Im\bar{3}m$-YH_6: a) temperature dependence of the electrical resistance $R(T)$ in the YH_6 (DAC K1) and YD_6 (DAC D1). Inset: the resistance drops to zero after cooling below T_C; b) temperature dependence of the electrical resistance in DAC M1. A ninefold decrease is observed. Inset: chamber of DAC M1 with Y sample and electrodes before and after the laser heating. c,d) Dependence of the electrical resistance on the external magnetic field (0–16 T) at 183 GPa and a current of 0.1 mA for even (c) and odd (d) values of the magnetic field. Due to the presence of several hydride phases in the sample, the superconducting transition in YH_6 can be observed as an upward feature of the R(T,H) curves due to the shunting effect in the fine-grained samples. The critical temperatures were determined at the onset of the resistance jump. e) The upper critical magnetic field was extrapolated using the Werthamer–Helfand–Hohenberg theory[24] and the Ginzburg–Landau[23] theory. f) The dependence of the critical temperature T_C (YH_6) on the applied magnetic field.

by spatial variations of the Ginzburg parameter ($\kappa = \lambda/\xi$) associated with fluctuations in the transition temperature T_C, so-called "dT_C-pinning" (or dk-pinning).

Analysis of the pinning force ($F_p = B \cdot I_C$) dependence on magnetic field (Figure S14a, Supporting Information) shows that according to Dew-Hughes[28] the dominant type of pinning in YH_6 is "dl-pinning." This allows us to extrapolate $I_C(T)$ data to low temperatures within the single vortex model $J_C = J_{c0}(1 - T/T_C)^{5/2}(1 + T/T_C)^{-1/2}$ which is suitable for rather low fields of several Tesla in the whole temperature range (see eq. (8) in ref. [29]). The extrapolation shows that at 4.2 K the critical current I_C in the sample can reach 1.75 A and the critical current density J_C may exceed 3500 A mm^{-2} (Figure 4c). However, using the Ginzburg–Landau model,[23] $J_C = J_{c0}(1 - T/T_C)^{3/2}$, gives lower values: the maximum critical current I_C in the sample ≈1 A, and the maximum critical current density J_C is about 2000 A mm^{-2} (Figure S14b, Supporting Information). These values of J_C are comparable with the parameters of commercial superconducting materials like NbTi and YBCO[30] (Figure 4d), which opens prospects of using superhydrides in electronic devices.

It is interesting to compare the experimentally obtained T_C with theoretical calculations based on the Bardeen–Cooper–Schrieffer[31–33] and the ME[34,35] theories. In early theoretical works, estimated T_C varies from 250 to 285 K,[1,15] (Figure S12, Supporting Information) which is quite far from the experimental values (224–226 K). Considering that the studied pressure range of 165–180 GPa has not been covered in previous papers, we carried out a series of calculations of the superconducting properties of $Im\bar{3}m$-YH_6 at a fixed pressure of 165 GPa (Tables S5–S8, Supporting Information) within the ME[34,35] approach, where the electron–electron Coulomb repulsion is accounted by one empirical parameter, the Coulomb pseudopotential μ^*, and a parameter-free superconducting density functional theory (SCDFT).[36,37]

Numerical solution of the isotropic ME equations[35] within the standard range of μ^* (cut-off frequency is 6 Ry) = 0.15–0.1 yields a T_C = 261–272 K, which is substantially higher than the experimental value for YH_6. This significant theoretical overestimation of the critical temperature calculated within the harmonic approach motivated us to include the effects of anharmonicity by performing calculations of the phonon band structure and Eliashberg function $\alpha^2F(\omega)$ using the stochastic self-consistent harmonic approximation (SSCHA)[38–40] (Figures S19–20,S27–28, Supporting Information), which is a nonperturbative variational method to consider anharmonic effects.

At a pressure of 165 GPa, the calculations with the anharmonic $\alpha^2F(\omega)$ show a decrease in the EPC coefficient of YH_6

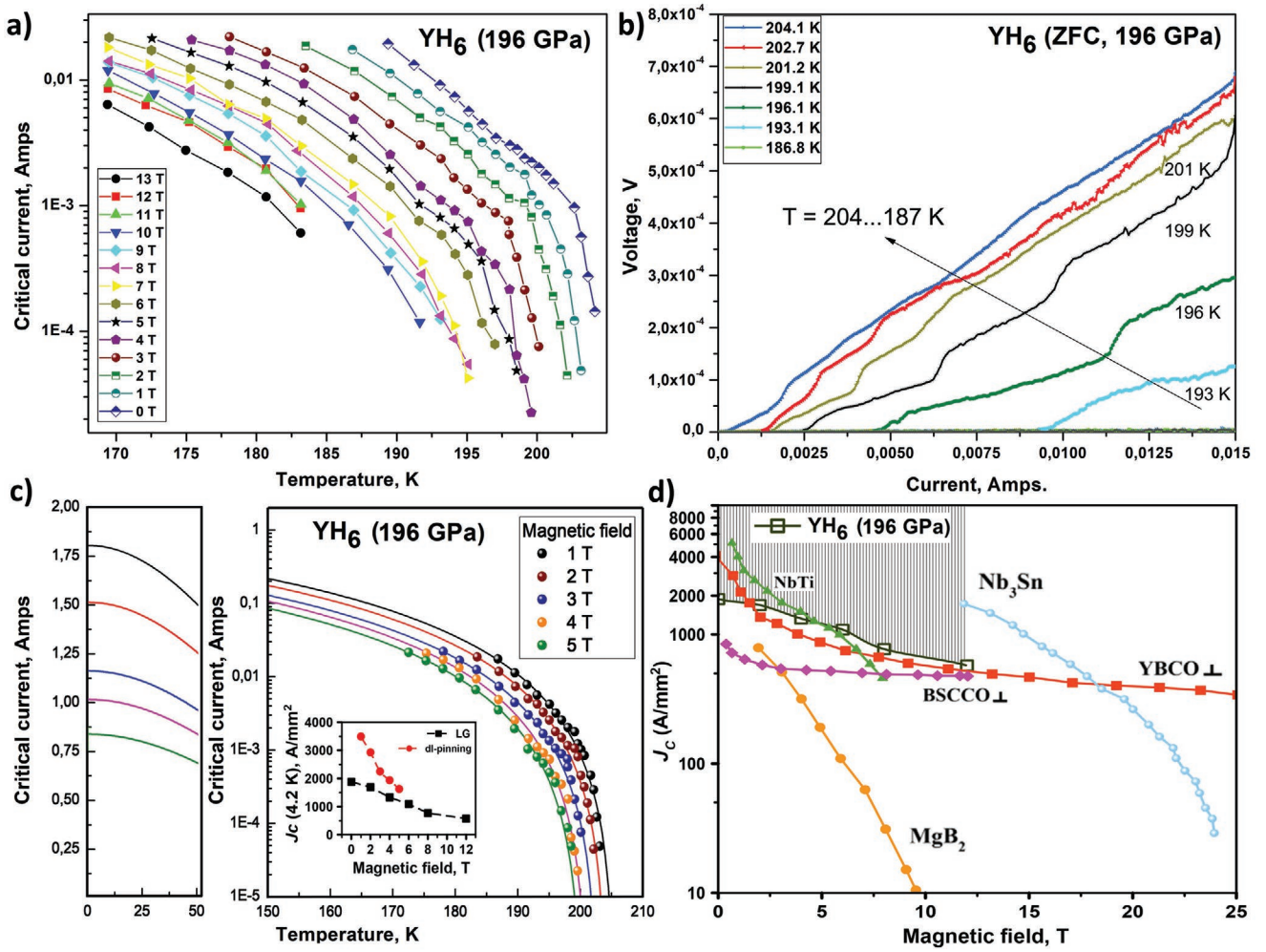

Figure 4. Dependence of the critical current on temperature and external magnetic fields (0–13 T) in $Im\bar{3}m$-YH_6 at 196 GPa. a) The critical current at different magnetic fields near T_C (defined below 50% resistance drop). b) The voltage–current characteristics of the YH_6 sample near T_C. c) Extrapolation of the temperature dependence of the critical current using the single vortex model[28] $J_C = J_{c0}(1 - T/T_C)^{5/2}(1 + T/T_C)^{-1/2}$; inset: dependencies of the critical current density at 4.2 K on the magnetic field. d) Critical current densities J_C of various industrial superconducting wires and of YH_6 (shaded area) at 4.2 K.[84] The lower bound of the critical current density of YH_6 was calculated assuming the maximum possible cross-section of the sample of 10×50 μm^2.

from 2.24 to 1.71 and an increase of ω_{log} from 929 to 1333 K due to hardening of the optical phonon modes. The overall influence of anharmonicity on the critical temperature is a decrease by 25 K, and resulting T_C is 236–247 K, which is still higher than the experimental values. To match the experimental data, including isotope coefficient $\alpha_{exp} = 0.4$, unusually high values of the Coulomb pseudopotential μ^*(6 Ry) = 0.19–0.22 are necessary. Estimations for YH_6 on the basis of DFT-calculated $N(E_F)$, λ, and ω_{log} give an expected upper critical magnetic field $\mu_0 H_C(0) \approx 60$ T, a superconducting gap of 48 meV, a coherence length $\xi_{BCS} = 0.5\sqrt{h/\pi e H_{c2}} = 23$ Å, and $N(E_F)(1 + \lambda) = 1.92$ (Table S5, Supporting Information).

The upper critical magnetic field $\mu_0 H_{c2}(0)$, found by extrapolation of the experimental data, exceeds 110 T (and can reach 158 T in the WHH model), which is more than 2–2.5 times higher than the value predicted within the BCS theory. In other words, the term $N(E_F)(1 + \lambda)$, related to the Sommerfeld constant, is at least four times higher than follows from DFT calculations, and ξ_{exp} is 14–17 Å. In this regard, it is curious that possible deviation from the ME theory of superconductivity in YH_6 was recently noted in ref. [41] on the basis of the T_C–T_F Uemura plot[42] for superhydrides. A similar disagreement, but less pronounced, is also observed for $Fm\bar{3}m$-LaH_{10},[2] where the $\mu_0 H_{c2}(0)$ exceeds the predicted one by ≈30–40%.

The SCDFT calculations, which incorporate the phonon-mediated pairing, mass renormalization, and pair-breaking Coulomb repulsion under the retardation effect without empirical parameters, such as μ^* in the ME equations, reveal another anomaly of YH_6. Solving the SCDFT gap equation with the anharmonic $\alpha^2F(\omega)$ (Equation (S1), Supporting Information) at 165 GPa yields $T_c = 160$ K and Coulomb potential $\mu = 0.187$, with an error bar of ≈2.5% originating from the random sampling step in solving the equation.[37,43] This value is about 100 K lower than the one found using the ME calculations and 64 K (≈28%) below the experimental value (224 K). A similar discrepancy has been reported in LaH_{10}[44] and within ab initio Eliashberg theory,[45] but

in those cases the difference was ≈20–30 K. Apart from this, the 64 K underestimation still indicates anomalously large impact of the Coulomb repulsion and implies something beyond the conventional phonon-mediated superconductivity that boosts the critical temperature up to the experimentally observed value.

Within the conventional mechanism, we can try to explain the discrepancy using at least two hypotheses. First, it could be achieved in the fully anisotropic Eliashberg equation.[46,47] In the work of Heil et al.,[15] at low temperatures the gap function showed a dispersion with a width of ≈30 meV, indicating that the pairing strength depends significantly on the band index and wavenumber. As seen in multiband superconductor MgB_2, averaging approaches using $\alpha^2F(\omega)$ generally yields smaller T_C's for systems with such band and wavenumber dependences.[48] Although the SCDFT gap equation presumably incorporates the effects included in the Eliashberg equations, they both can give a little different T_C values, as has been pointed out for LaH_{10}.[47] Also, large phonon energy scales in the hydride could give relevance higher order EPC effects beyond the Born–Oppenheimer and the Migdal approximations. Second, as Sano et al.[49] demonstrated, in superconducting sulfur hydride H_3S, the Debye–Waller correction[50] to the electronic band structure (including the finite spread of the ionic sites) and the vertex correction (including the higher order perturbation of the self-energy due to the electron–phonon interaction) both change the calculated value of T_C by several tens of Kelvin. It would be interesting to explore such effects in YH_6.

In this study, the novel high-T_C superconductor $Im\bar{3}m$-YH_6 was discovered together with $I4/mmm$-YH_4 and YH_7 at pressures of 160–196 GPa, confirming theoretical predictions.[1] The low-symmetry molecular yttrium hydride $P1$-YH_{7+x} ($x = \pm 0.5$) was found to cause complex XRD patterns at 166 GPa. The measured critical temperature of $Im\bar{3}m$-YH_6 is 224 K, which is unexpectedly lower than the theoretically predicted value (>273 K).[10] The extrapolated upper critical magnetic field $\mu_0 H_{C2}(0)$ = 116–158 T is more than two times larger than the calculated one (≈60 T). Electrical transport measurements show that the critical current density J_C in our samples may exceed 3500 A mm^{-2} at 0 K, which is remarkable in comparison with currently known and used superconductors.

Anharmonic effects in $Im\bar{3}m$-YH_6 lead to a decrease in the EPC coefficient from 2.24 to 1.71 and lowering the critical temperature by 25 K. An anomalously large impact of the Coulomb repulsion was found in yttrium hexahydride within both the ME and the SCDFT approaches. The calculated T_C agreed with the experimental critical temperature and the isotope coefficient only when the Coulomb pseudopotential μ^*(6 Ry) was equal to 0.19–0.22 and anharmonicity is included in the calculations. The parameter-free SCDFT calculations for YH_6 give substantially lower T_C = 160 K which implies inaccuracy of SCDFT in its current form for this compound, and again suggests the importance of effects missing in the conventional ME theory.

Methods Section

Experimental Details: To perform this experimental study, three DACs—K1, M1, and M3—were loaded. The diameter of the working surface of the diamond anvils was 280 μm beveled at an angle of 8.5° to a culet of 50 μm. The XRD patterns of all samples in the DACs were recorded at the GSECARS synchrotron beamline at the Advanced Photon Source (APS), Argonne, U.S. An X-ray beam with an energy of 42 and 37 keV and wavelength λ = 0.295 and 0.334 Å was focused to 2.5 × 3.5 μm. A Pilatus 1M CdTe detector was placed at a distance of ≈200 mm from the sample. The exposure time was 20–60 s. LaB_6 standard was used for the detector geometry calibration. The XRD data were analyzed and integrated using Dioptas software package (version 0.4).[51] The full profile analysis of the diffraction patterns and the calculation of the unit cell parameters were performed in JANA2006 computing system[52] using the Le Bail method.[53]

The heating of the sample was performed at GSECARS by ≈10^5 pulses of a Nd:YAG infrared laser with a wavelength λ = 1.064 μm, the duration of each pulse was 1 μs.[54] The temperature measurements were carried out using the gray body radiation fit within the Planck function at the laser heating system of the GSECARS beamline of the APS. The applied pressure was measured by the edge position of the Raman signal of diamond[55] using Acton SP2500 spectrometer with PIXIS:100 spectroscopic-format CCD.[56] The pressure in the DACs was determined by the Raman signal of diamond.[57]

Deuterated ammonium borane (d-AB) was synthesized from $NaBD_4$ (98% D, Sigma Aldrich) via the reaction with ammonium formate $HCOONH_4$ in tetrahydrofuran followed by isotopic substitution (H→D) in D_2O.[58] After removing of solvents and vacuum drying, the obtained ND_3BD_3 was analyzed by ^{1}H NMR and Raman spectroscopy. Deuterium content in the product was found to be 92%. Partially substituted NH_3BD_3 and ND_3BH_3 might be synthesized in a similar way for later use as a source of HD.

Magnetotransport measurements were performed on samples with at least two hydride phases and, therefore, the voltage contacts of the Van der Pauw scheme might be connected to low-T_C phase. As a result, the superconducting transition in YH_6 could be observed as an upward feature of the R(T,H) curves due to the shunting effect in the fine-grained samples as described in Figure S17 in the Supporting Information (see also refs. [59,60]).

For the Dew-Hughes model[28] of the pinning force $f \approx h^p(1-h)^q$, the parameters should be p = 0.5, q = 2, h_{max} = 0.2, which was close to the fit of the experimental data (Figure S14a, Supporting Information). Depinning critical current for this type of pinning could be described within the single vortices model, where vortices were pinned on randomly distributed weak pinning centers via spatial fluctuations of the charge carrier mean free path, or in other words "*dl*-pinning."

To prove superconducting properties of YH_6 samples, an attempt was made to detect the Meissner effect—the expulsion of magnetic flux from the material. Previously, this effect was measured only once on a sample of H_3S with a diameter of ≈100 μm.[61,62] However, these typical yttrium hexahydride samples were much smaller (Table 2, 9–15 μm), that made problematic magnetization measurements by both a superconducting quantum interference device (SQUID) magnetometer as well as AC magnetic susceptibility method due to the small sample volume.

Computational Details: The computational predictions of the thermodynamic stability of the Y–H phase at 150, 200, and 250 GPa were carried out using the variable-composition evolutionary algorithm USPEX.[16–18] The first generation consisting of 120 structures was produced using random symmetric[18] and random topology[63] generators, whereas all subsequent generations contained 20% of random structures and 80% of those created using heredity, softmutation, and transmutation operators. The evolutionary searches were combined with structure relaxations using the DFT[64,65] within the Perdew–Burke–Ernzerhof functional (generalized gradient approximation)[66] and the projector augmented wave method[67,68] as implemented in the VASP code.[69–71] The kinetic energy cutoff for plane waves was 600 eV. The Brillouin zone was sampled using the Γ-centered k-points meshes with a resolution of $2\pi \times 0.05$ Å^{-1}. The methodology was similar to those used in the previous works.[8,72]

The equations of state of the discovered YH_4, YH_6, and YH_7 phases were calculated using the same methods with the plane wave kinetic energy cutoff set to 700 eV. The phonon densities of states of the studied

Table 3. Detailed conditions for calculating T_c of YH_6 within the SCDFT approach.

Crystal structure setting		$(YH_6)_2$ simple cubic
Charge density	k	$12 \times 12 \times 12$ equal mesh
	Interpolation	First-order Hermite Gaussian[83] with a width of 0.020 Ry
Dielectric matrix ε	k for bands crossing E_F	$15 \times 15 \times 15$ equal mesh
	k for other bands	$5 \times 5 \times 5$ equal mesh
	Number of unoccupied bands[a)]	82
	Interpolation	Tetrahedron with the Rath–Freeman treatment[85]
	Cutoff	12.8 Ry
DOS for phononic kernels	k	$19 \times 19 \times 19$ equal mesh
	Interpolation	Tetrahedron with the Blöchl correction[67]
SCDFT gap function	Number of unoccupied bands[b)]	82
	k for the electronic kernel	$5 \times 5 \times 5$ equal mesh
	k for the KS energies	$19 \times 19 \times 19$ equal mesh
	Sampling points for bands crossing E_F	6000
	Sampling points for other bands	200
	Sampling error in T_c, %	≈2.5

[a)]States up to $E_F + 70$ eV are taken into account; [b)]States up to $E_F + 70$ eV are taken into account.

materials were also calculated using the finite displacements method (VASP and PHONOPY).[73,74]

The calculations of superconducting T_C were carried out using QUANTUM ESPRESSO (QE) package.[75,76] The phonon frequencies and EPC coefficients were computed using density functional perturbation theory,[77] employing the plane-wave pseudopotential method and Perdew–Burke–Ernzerhof exchange-correlation functional.[66] In ab initio calculations of the EPC coefficient λ, the first Brillouin zone was sampled using a $3 \times 3 \times 3$ or $4 \times 4 \times 4$ q-points mesh and a denser $16 \times 16 \times 16$ k-points mesh (with the Gaussian smearing and $\sigma = 0.005$ Ry, which approximates the zero-width limits in the calculation of λ) for YH_7 and YH_4.

The calculations of the Eliashberg function of $Im\bar{3}m$-YH_6 were performed using $6 \times 6 \times 6$ q-points and $60 \times 60 \times 60$ k-points meshes. T_C was calculated by solving the isotropic Eliashberg equations[35] using the iterative self-consistent method for the imaginary part of the order parameter $\Delta(T, \omega)$ (superconducting gap) and the renormalization wave function $Z(T, \omega)$ assuming that the Coulomb repulsion between the electrons could be parametrized with μ^*. More approximate estimates of T_C were made using the Allen–Dynes formula.[78]

The superconducting transition temperature T_C of YH_6 was also calculated by solving the gap equation in the DFT for superconductors (SCDFT)[36,37]

$$\Delta_{nk}(T) = -Z_{nk}(T)\Delta_{nk}(T) - \frac{1}{2}\sum_{n'k'} K_{nkn'k'}(T)\frac{\tanh\beta E_{n'k'}}{E_{n'k'}}\Delta_{n'k'}(T) \quad (1)$$

with $E_{n'k'} = \sqrt{\xi^2_{n'k'} + \Delta^2_{n'k'}}$. Solving this equation for different temperatures $\beta = 1/T$, it was seen that the order parameter $\Delta_{n'k'}$ had a nonzero solution below any threshold temperature, which was identified as T_c. Labels n, n', k, and k' indicate the Kohn–Sham band and crystal wave number indices, respectively. ξ_{nk} is the energy eigenvalue of state nk from the Fermi level, as calculated using the standard Kohn–Sham equation for the normal state. The kernels of the gap equation $Z_{nk}(T)$ and $K_{nkn'k'}(T)$ represent the electron–phonon and electron–electron Coulomb interaction effects, the formulas for which (see paper by Kruglov et al. [44], which is based on the method described in refs. [36,37,79,80]) had been constructed so that the perturbation effects, almost the same as those in the Eliashberg equations with the Migdal approximation,[34,35,81,82] were included. The solution of Equation (S1) in the Supporting Information required preprocessing to calculate the dielectric matrix for the screened electron–electron Coulomb interaction within the random phase approximation[83] and the electronic density of states (DOS) for the normal state. The detailed conditions for the SCDFT calculation are summarized in **Table 3**. The anharmonic calculations, including the vibrational contribution to the enthalpy, were performed using the SSCHA.[38] The anharmonic force constant matrices of $Im\bar{3}m$-YH_6 were obtained by calculating the forces in $3 \times 3 \times 3$ supercells and combined with the DFPT electron–phonon calculations performed in a fine $12 \times 12 \times 12$ mesh to calculate the anharmonic Eliashberg function $\alpha^2F(\omega)$.

Supporting Information

Supporting Information is available from the Wiley Online Library or from the author.

Acknowledgements

The work on the high-pressure experiments was supported by the Ministry of Science and Higher Education of the Russian Federation within the state assignment of the FSRC "Crystallography and Photonics" of RAS and by the Russian Science Foundation (project no. 19-12-00414). A.G.G. acknowledges the use of the facilities of the Center for Collective Use "Accelerator Center for Neutron Research of the Structure of Substance and Nuclear Medicine" of the INR RAS. A.G.K. thanks the Russian Foundation for Basic Research (project no. 19-03-00100) for the financial support of this work. A.R.O., D.V.S., and A.G.K. thank the Russian Science Foundation (grant 19-72-30043). The reported study was funded by the RFBR, project 20-32-90099. A.R.O and D.V.S. thank the Ministry of Science and Higher Education agreement No. 075-15-2020-808. Portions of this work were performed at GeoSoilEnviroCARS (The University of Chicago, Sector 13), Advanced Photon Source (APS), Argonne National Laboratory. GeoSoilEnviroCARS was supported by the National Science Foundation—Earth Sciences (EAR-1634415) and Department of Energy—GeoSciences (DE-FG02-94ER14466). Use of the GSECARS Raman Lab System was supported by the NSF MRI Proposal (EAR-1531583). This research used the resources of the Advanced Photon Source, a U.S. Department of Energy (DOE) Office of Science User Facility operated for the DOE Office of Science by Argonne National Laboratory under contract no. DE-AC02-06CH11357 and R.B. acknowledges the support from the European Research Council (ERC) under the European Union's Horizon 2020 research and innovation programme (grant agreement no. 802533). R.B. thankfully acknowledges the computer resources at Altamira and the technical support provided by Physics Institute of Cantabria (IFCA) (RES-FI-2020-3-0028). The research used resources of the LPI Shared Facility Center. A.V.S., O.A.S. and V.M.P. acknowledge support of the state assignment of the Ministry of Science and Higher Education of the Russian Federation (Project No. 0023-2019-0005). A.B. acknowledges financial support from the Spanish Ministry of Science and Innovation (PID2019-105488GB-I00). R.A. performed the calculations at the Supercomputer Center at the Institute for Solid State Physics in the University of Tokyo. The authors thank Igor Grishin (Skoltech) for proofreading of the manuscript.

Conflict of Interest

The authors declare no conflict of interest.

Author Contributions

I.A.T., D.V.S., and A.G.K. contributed equally to this work. D.V.S., I.A.T, A.G.I., A.G.G., V.B.P., E.G., V.V.S. performed the experiment. I.A.T. deposited electrodes and performed the superconductivity measurements. A.V.S., O.A.S., V.M.P. performed the magnetotransport experiments in high magnetic fields and participated in data processing and discussions. A.G.K. and A.R.O. prepared the theoretical analysis. A.B., I.E., R.B., M.C., F.M., L.M. calculated the anharmonic phonon density of states and Eliashberg function. R.A. performed the calculations of T_C within the SCDFT formalism. D.V.S., A.G.K., A.R.O. wrote the manuscript. All authors provided critical feedback and helped shape the research, analysis, and manuscript.

Data Availability Statement

The data that support the findings of this study are available from the corresponding author upon reasonable request.

Keywords

Bardeen–Cooper–Schrieffer theory, Migdal–Eliashberg theory, pressure-stabilized hydrides, superconductivity, yttrium hydrides, yttrium hexahydride

Received: October 8, 2020
Revised: December 25, 2020
Published online: March 10, 2021

[1] H. Liu, I. I. Naumov, R. Hoffmann, N. W. Ashcroft, R. J. Hemley, *Proc. Natl. Acad. Sci. USA* **2017**, *114*, 6990.
[2] A. P. Drozdov, P. P. Kong, V. S. Minkov, S. P. Besedin, M. A. Kuzovnikov, S. Mozaffari, L. Balicas, F. F. Balakirev, D. E. Graf, V. B. Prakapenka, E. Greenberg, D. A. Knyazev, M. Tkacz, M. I. Eremets, *Nature* **2019**, *569*, 528.
[3] M. Somayazulu, M. Ahart, A. K. Mishra, Z. M. Geballe, M. Baldini, Y. Meng, V. V. Struzhkin, R. J. Hemley, *Phys. Rev. Lett.* **2019**, *122*, 027001.
[4] V. Struzhkin, B. Li, C. Ji, X.-J. Chen, V. Prakapenka, E. Greenberg, I. Troyan, A. Gavriliuk, H. Mao, *Matter Radiat. Extremes* **2020**, *5*, 028201.
[5] E. Snider, N. Dasenbrock-Gammon, R. McBride, M. Debessai, H. Vindana, K. Vencatasamy, K. V. Lawler, A. Salamat, R. P. Dias, *Nature* **2020**, *586*, 373.
[6] W. Chen, D. V. Semenok, A. G. Kvashnin, I. A. Kruglov, M. Galasso, H. Song, X. Huang, D. Duan, A. F. Goncharov, V. B. Prakapenka, A. R. Oganov, T. Cui, *Nat. Commun.* **2021**, *12*, 273.
[7] D. V. Semenok, A. G. Kvashnin, A. G. Ivanova, V. Svitlyk, V. Y. Fominski, A. V. Sadakov, O. A. Sobolevskiy, V. M. Pudalov, I. A. Troyan, A. R. Oganov, *Mater. Today* **2020**, *33*, 36.
[8] A. G. Kvashnin, D. V. Semenok, I. A. Kruglov, I. A. Wrona, A. R. Oganov, *ACS Appl. Mater. Interfaces* **2018**, *10*, 43809.
[9] I. A. Kruglov, A. G. Kvashnin, A. F. Goncharov, A. R. Oganov, S. S. Lobanov, N. Holtgrewe, S. Jiang, V. B. Prakapenka, E. Greenberg, A. V. Yanilkin, *Sci. Adv.* **2018**, *4*, eaat9776.
[10] N. P. Salke, M. M. D. Esfahani, Y. Zhang, I. A. Kruglov, J. Zhou, Y. Wang, E. Greenberg, V. B. Prakapenka, J. Liu, A. R. Oganov, J.-F. Lin, *Nat. Commun.* **2019**, *10*, 4453.
[11] D. Zhou, D. V. Semenok, D. Duan, H. Xie, W. Chen, X. Huang, X. Li, B. Liu, A. R. Oganov, T. Cui, *Sci. Adv.* **2020**, *6*, eaax6849.
[12] D. Zhou, D. V. Semenok, H. Xie, X. Huang, D. Duan, A. Aperis, P. M. Oppeneer, M. Galasso, A. I. Kartsev, A. G. Kvashnin, A. R. Oganov, T. Cui, *J. Am. Chem. Soc.* **2020**, *142*, 2803.
[13] Y. Li, J. Hao, H. Liu, J. S. Tse, Y. Wang, Y. Ma, *Sci. Rep.* **2015**, *5*, 09948.
[14] K. S. Grishakov, N. N. Degtyarenko, E. A. Mazur, *J. Exp. Theor. Phys.* **2019**, *128*, 105.
[15] C. Heil, S. di Cataldo, G. B. Bachelet, L. Boeri, *Phys. Rev. B* **2019**, *99*, 220502.
[16] A. R. Oganov, C. W. Glass, *J. Chem. Phys.* **2006**, *124*, 244704.
[17] A. R. Oganov, A. O. Lyakhov, M. Valle, *Acc. Chem. Res.* **2011**, *44*, 227.
[18] A. O. Lyakhov, A. R. Oganov, H. T. Stokes, Q. Zhu, *Comput. Phys. Commun.* **2013**, *184*, 1172.
[19] *Dynamical Theory of Crystal Lattices*, Oxford University Press, Oxford, UK **1998**.
[20] A. R. Oganov, Y. Ma, A. O. Lyakhov, M. Valle, C. Gatti, *Rev. Mineral. Geochem.* **2010**, *71*, 271.
[21] P. P. Kong, V. S. Minkov, M. A. Kuzovnikov, S. P. Besedin, A. P. Drozdov, S. Mozaffari, L. Balicas, F. F. Balakirev, V. B. Prakapenka, E. Greenberg, D. A. Knyazev, M. I. Eremets, arXiv:1909.10482 **2019**.
[22] a) R. P. Dias, E. Snider, N. Dasenbrock-Gammon, R. McBride, in *Bulletin of the American Physical Society*, American Physical Society, Washington, DC **2020**; b) E. Snider, N. Dasenbrock-Gammon, R. McBride, X. Wang, N. Meyers, K. V. Lawler, E. Zurek, A. Salamat, R. Dias, arXiv:2012.13627 **2020**.
[23] V. L. Ginzburg, L. D. Landau, *Zh. Eksp. Teor. Fiz.* **1950**, *20*, 1064.
[24] N. R. Werthamer, E. Helfand, P. C. Hohenberg, *Phys. Rev.* **1966**, *147*, 295.
[25] T. Baumgartner, M. Eisterer, H. W. Weber, R. Flükiger, C. Scheuerlein, L. Bottura, *Supercond. Sci. Technol.* **2013**, *27*, 015005.
[26] J. P. Carbotte, *Rev. Mod. Phys.* **1990**, *62*, 1027.
[27] A. P. Drozdov, M. I. Eremets, I. A. Troyan, V. Ksenofontov, S. I. Shylin, *Nature* **2015**, *525*, 73.
[28] D. Dew-Hughes, *Philos. Mag. (1798-1977)* **1974**, *30*, 293.
[29] R. Griessen, W. Hai-hu, A. J. J. van Dalen, B. Dam, J. Rector, H. G. Schnack, S. Libbrecht, E. Osquiguil, Y. Bruynseraede, *Phys. Rev. Lett.* **1994**, *72*, 1910.
[30] J. Schwartz, F. Hunte, W. K. Chan, X. F. Gou, X. T. Liu, M. Phillips, Q. V. Le, G. Naderi, M. Turenne, L. Ye, arXiv:1108.1634, **2011**.
[31] L. N. Cooper, *Phys. Rev.* **1956**, *104*, 1189.
[32] J. Bardeen, L. N. Cooper, J. R. Schrieffer, *Phys. Rev.* **1957**, *106*, 162.
[33] J. Bardeen, L. N. Cooper, J. R. Schrieffer, *Phys. Rev.* **1957**, *108*, 1175.
[34] A. B. Migdal, *J. Exp. Theor. Phys.* **1958**, *34*, 996.
[35] G. M. Eliashberg, *J. Exp. Theor. Phys.* **1959**, *11*, 696.
[36] M. Lüders, M. A. L. Marques, N. N. Lathiotakis, A. Floris, G. Profeta, L. Fast, A. Continenza, S. Massidda, E. K. U. Gross, *Phys. Rev. B* **2005**, *72*, 024545.
[37] M. A. L. Marques, M. Lüders, N. N. Lathiotakis, G. Profeta, A. Floris, L. Fast, A. Continenza, E. K. U. Gross, S. Massidda, *Phys. Rev. B* **2005**, *72*, 024546.
[38] I. Errea, M. Calandra, F. Mauri, *Phys. Rev. B* **2014**, *89*, 064302.
[39] R. Bianco, I. Errea, L. Paulatto, M. Calandra, F. Mauri, *Phys. Rev. B* **2017**, *96*, 014111.
[40] L. Monacelli, I. Errea, M. Calandra, F. Mauri, *Phys. Rev. B* **2018**, *98*, 024106.
[41] E. F. Talantsev, *Supercond. Sci. Technol.* **2020**, *33*, 124001.
[42] Y. J. Uemura, *Phys. Rev. Mater.* **2019**, *3*, 104801.
[43] R. Akashi, K. Nakamura, R. Arita, M. Imada, *Phys. Rev. B* **2012**, *86*, 054513.
[44] I. A. Kruglov, D. V. Semenok, H. Song, R. Szczęśniak, I. A. Wrona, R. Akashi, M. M. D. Esfahani, D. Duan, T. Cui, A. G. Kvashnin, A. R. Oganov, *Phys. Rev. B* **2020**, *101*, 024508.
[45] A. Sanna, J. A. Flores-Livas, A. Davydov, G. Profeta, K. Dewhurst, S. Sharma, E. K. U. Gross, *J. Phys. Soc. Jpn.* **2018**, *87*, 041012.
[46] E. R. Margine, F. Giustino, *Phys. Rev. B* **2013**, *87*, 024505.
[47] I. Errea, F. Belli, L. Monacelli, A. Sanna, T. Koretsune, T. Tadano, R. Bianco, M. Calandra, R. Arita, F. Mauri, J. A. Flores-Livas, *Nature* **2020**, *578*, 66.

[48] H. J. Choi, D. Roundy, H. Sun, M. L. Cohen, S. G. Louie, *Phys. Rev. B* **2002**, *66*, 020513.
[49] W. Sano, T. Koretsune, T. Tadano, R. Akashi, R. Arita, *Phys. Rev. B* **2016**, *93*, 094525.
[50] M. Yussouff, B. K. Rao, P. Jena, *Solid State Commun.* **1995**, *94*, 549.
[51] C. Prescher, V. B. Prakapenka, *High Pressure Res.* **2015**, *35*, 223.
[52] V. Petříček, M. Dušek, L. Palatinus, *Z. Kristallogr. - Cryst. Mater.* **2014**, *229*, 345.
[53] A. L. Bail, *Powder Diffr.* **2005**, *20*, 316.
[54] V. B. Prakapenka, A. Kubo, A. Kuznetsov, A. Laskin, O. Shkurikhin, P. Dera, M. L. Rivers, S. R. Sutton, *High Pressure Res.* **2008**, *28*, 225.
[55] Y. Akahama, H. Kawamura, *J. Phys.: Conf. Ser.* **2010**, *215*, 012195.
[56] N. Holtgrewe, E. Greenberg, C. Prescher, V. B. Prakapenka, A. F. Goncharov, *High Pressure Res.* **2019**, *39*, 457.
[57] M. I. Eremets, *J. Raman Spectrosc.* **2003**, *34*, 515.
[58] V. M. Parvanov, G. K. Schenter, N. J. Hess, L. L. Daemen, M. Hartl, A. C. Stowe, D. M. Camaioni, T. Autrey, *Dalton Trans.* **2008**, 4514.
[59] S. C. Ems, J. C. Swihart, *Phys. Lett. A* **1971**, *37*, 255.
[60] S. V. Postolova, A. Y. Mironov, M. R. Baklanov, V. M. Vinokur, T. I. Baturina, *Sci. Rep.* **2017**, *7*, 1718.
[61] I. Troyan, A. Gavriliuk, R. Rüffer, A. Chumakov, A. Mironovich, I. Lyubutin, D. Perekalin, A. P. Drozdov, M. I. Eremets, *Science* **2016**, *351*, 1303.
[62] X. Huang, X. Wang, D. Duan, B. Sundqvist, X. Li, Y. Huang, H. Yu, F. Li, Q. Zhou, B. Liu, T. Cui, *Natl. Sci. Rev.* **2019**, *6*, 713.
[63] P. V. Bushlanov, V. A. Blatov, A. R. Oganov, *Comput. Phys. Commun.* **2019**, *236*, 1.
[64] P. Hohenberg, W. Kohn, *Phys. Rev.* **1964**, *136*, B864.
[65] W. Kohn, L. J. Sham, *Phys. Rev.* **1965**, *140*, A1133.
[66] J. P. Perdew, K. Burke, M. Ernzerhof, *Phys. Rev. Lett.* **1996**, *77*, 3865.
[67] P. E. Blöchl, *Phys. Rev. B* **1994**, *50*, 17953.
[68] G. Kresse, D. Joubert, *Phys. Rev. B* **1999**, *59*, 1758.
[69] G. Kresse, J. Furthmüller, *Phys. Rev. B* **1996**, *54*, 11169.
[70] G. Kresse, J. Hafner, *Phys. Rev. B* **1993**, *47*, 558.
[71] G. Kresse, J. Hafner, *Phys. Rev. B* **1994**, *49*, 14251.
[72] D. V. Semenok, A. G. Kvashnin, I. A. Kruglov, A. R. Oganov, *J. Phys. Chem. Lett.* **2018**, *9*, 1920.
[73] A. Togo, I. Tanaka, *Scr. Mater.* **2015**, *108*, 1.
[74] A. Togo, F. Oba, I. Tanaka, *Phys. Rev. B* **2008**, *78*, 134106.
[75] P. Giannozzi, S. Baroni, N. Bonini, M. Calandra, R. Car, C. Cavazzoni, D. Ceresoli, G. L. Chiarotti, M. Cococcioni, I. Dabo, A. D. Corso, S. de Gironcoli, S. Fabris, G. Fratesi, R. Gebauer, U. Gerstmann, C. Gougoussis, A. Kokalj, M. Lazzeri, L. Martin-Samos, N. Marzari, F. Mauri, R. Mazzarello, S. Paolini, A. Pasquarello, L. Paulatto, C. Sbraccia, S. Scandolo, G. Sclauzero, A. P. Seitsonen, et al., *J. Phys.: Condens. Matter* **2009**, *21*, 395502.
[76] P. Giannozzi, O. Andreussi, T. Brumme, O. Bunau, M. B. Nardelli, M. Calandra, R. Car, C. Cavazzoni, D. Ceresoli, M. Cococcioni, N. Colonna, I. Carnimeo, A. D. Corso, S. de Gironcoli, P. Delugas, R. A. DiStasio, A. Ferretti, A. Floris, G. Fratesi, G. Fugallo, R. Gebauer, U. Gerstmann, F. Giustino, T. Gorni, J. Jia, M. Kawamura, H.-Y. Ko, A. Kokalj, E. Küçükbenli, M. Lazzeri, et al., *J. Phys.: Condens. Matter* **2017**, *29*, 465901.
[77] S. Baroni, S. de Gironcoli, A. Dal Corso, P. Giannozzi, *Rev. Mod. Phys.* **2001**, *73*, 515.
[78] P. B. Allen, R. C. Dynes, *Phys. Rev. B* **1975**, *12*, 905.
[79] R. Akashi, R. Arita, *Phys. Rev. B* **2013**, *88*, 014514.
[80] R. Akashi, M. Kawamura, S. Tsuneyuki, Y. Nomura, R. Arita, *Phys. Rev. B* **2015**, *91*, 224513.
[81] D. J. Scalapino, in *Superconductivity: Part 1 (In Two Parts)* (Ed: R. D. Parks), Dekker, New York **1969**.
[82] J. R. Schrieffer, *Theory Of Superconductivity*, Perseus Books, Reading, MA, USA **1999**.
[83] D. Pines, *Elementary Excitations in Solids : Lectures on Phonons, Electrons, and Plasmons*, Perseus Books, Reading, MA **1999**.
[84] Plots – MagLab, https://nationalmaglab.org/magnet-development/applied-superconductivity-center/plots (accessed: January 2021).
[85] J. Rath, A. J. Freeman, *Phys. Rev. B* **1975**, *11*, 2109.